C. R. Acad. Sci. Paris, Sciences de la Terre et des planètes / Earth and Planetary Sciences 333 (2001) 483–494

S1251-8050(01)01668-8/FLA

Tectonique / Tectonics

Long-term slip rates and characteristic slip: keys to active fault behaviour and earthquake hazard

Paul Tapponnier[a,*], Frederick James Ryerson[b], Jerome Van der Woerd[a,b], Anne-Sophie Mériaux[a,b], Cécile Lasserre[a]

[a] Institut de physique du Globe de Paris, 4, place Jussieu, 75252 Paris cedex 05, France
[b] IGPP, Lawrence Livermore National Laboratory, Livermore, CA 94550, USA

Received 16 July 2001; accepted 28 August 2001

Abstract – Over periods of thousands of years, active faults tend to slip at constant rates. Pioneer studies of large Asian faults show that cosmogenic radionuclides (^{10}Be, ^{26}Al) provide an unparalleled tool to date surface features, whose offsets yield the longest records of recent cumulative movement. The technique is thus uniquely suited to determine long-term (10–100 ka) slip rates. Such rates, combined with coseismic slip-amounts, can give access to recurrence times of earthquakes of similar sizes. Landform dating – morphochronology – is therefore essential to understand fault-behaviour, evaluate seismic hazard, and build physical earthquake models. It is irreplaceable because long-term slip-rates on interacting faults need not coincide with GPS-derived, interseismic rates, and can be difficult to obtain from paleo-seismological trenching. © 2001 Académie des sciences / Éditions scientifiques et médicales Elsevier SAS

cosmogenic dating / active faults of Asia / sliprates / characteristic slip / earthquake recurrence and hazard

Résumé – Vitesses de glissement à long terme et dislocations cosismiques caractéristiques : clés du fonctionnement des failles actives et de l'aléa sismique. La vitesse de glissement moyenne des failles actives tend à être constante sur des périodes longues de quelques milliers d'années. L'étude systématique des grandes failles actives de l'Asie démontre que les radionuclides cosmogéniques (^{10}Be, ^{26}Al) sont un outil exceptionnel pour dater les marqueurs géomorphologiques superficiels, dont les décalages fournissent le meilleur enregistrement à long terme des mouvements cumulés résultant de la répétition des séismes. Cette technique est donc la plus efficace pour déterminer les vitesses de glissement sur des échelles de temps de 10 000 à 100 000 ans. Combinées aux valeurs des glissements cosismiques, ces vitesses donnent accès au temps de récurrence de séismes de taille semblable. L'approche « morphochronologique » est donc essentielle pour comprendre et modéliser physiquement le fonctionnement des failles ainsi que pour évaluer l'aléa sismique. Elle est irremplaçable, car les vitesses de glissement à long terme sur des failles qui interagissent ne coïncident pas nécessairement avec les vitesses inter-sismiques déduites des mesures de géodésie spatiale. Par ailleurs, de telles vitesses sont généralement difficiles à obtenir à partir de tranchées paléosismologiques. © 2001 Académie des sciences / Éditions scientifiques et médicales Elsevier SAS

datation par isotopes cosmogéniques / failles actives d'Asie / vitesse de glissement / glissement caractéristique / temps de récurrence / risque sismique

* Correspondence and reprints.
E-mail address: tappon@ipgp.jussieu.fr (P. Tapponnier).

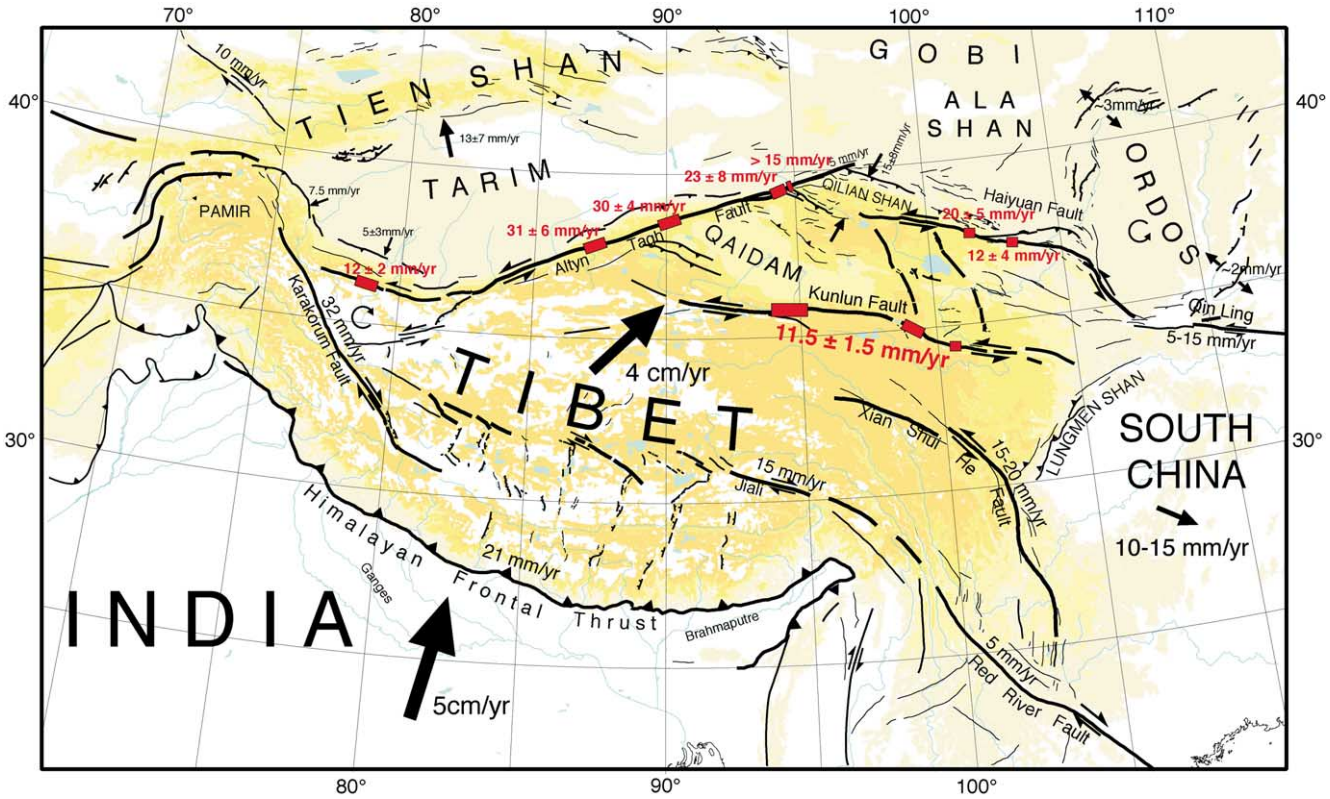

Figure 1. Kinematic map of active faults in Tibet. Red boxes are location of sites where slip rates have been determined by dating geomorphic offsets of alluvial terraces or moraines.

Figure 1. Carte cinématique des failles actives du Tibet. Les rectangles rouges indiquent les sites ou ensembles de sites où la vitesse de mouvement a été déterminée par des datations de marqueurs géomorphologiques décalés, tels que des terrasses alluviales ou des moraines.

1. Introduction

On many active faults of the world, the most valuable, and often missing, quantitative piece of information is an accurate, long-term slip rate. Together with the amount of coseismic slip, it governs the seismic cycle. Geodetic techniques give access to short-term, essentially instantaneous rates that include both inter- and post-seismic deformation. Such instantaneous rates need not coincide with long term block motions, especially in regions where blocks are small and faults between them interact. At the other extreme, plate-tectonic models typically provide boundary rates that may encompass several faults and smooth out motions over millions of years. The time scale that is most relevant to understand fault behaviour and earthquake recurrence, hence seismic hazard, lies between these extremes.

In situ geological studies can provide average slip-rates over periods thousands of years long, enough to span a large number of seismic cycles, whose duration in continents is typically greater than a few hundred years (e.g., [8, 14, 26]). Yet, even on a fault as extensively studied as California's San Andreas, only two well-constrained, direct determinations of the millennial slip-rate exist, at Wallace Creek and Cajon Pass (e.g., [19, 25]). There are several reasons for such dearth. First, ground trenching is better adapted at detecting paleo-earthquakes than at studying large cumulative offsets, particularly on strike-slip faults. The best record of long-term horizontal offsets is usually preserved by surface landforms along the fault-trace, but sites with well-defined markers must be found. Finally and most importantly, it has been difficult so far to date offset geomorphic surfaces.

To determine fault-slip rates over thousands or tens of thousands of years, test the hypothesis that certain earthquakes repeat with characteristic slip on given fault patches, and thus improve understanding of fault behaviour and seismic hazard, accurate measurement and dating of surface offsets, small and large, are necessary. Exploiting the new surface dating opportunity offered by cosmogenic isotopes (^{10}Be, ^{26}Al), we have started to quantify, systematically, offset landforms along large active faults in Asia (*figure 1*). We illustrate here the use of the technique to constrain the rate of slip on Tibet's Kunlun fault over a length of hundreds of kilometres and a time span of several ten thousand years (*figures 2–5*). We also show that characteristic slip tends to occur during large earth-

quakes on two segments of the fault. The average recurrence time of such repeated events can thus be estimated. The same approach is beginning to yield similar results on other Central Asian strike-slip faults, and should be applicable elsewhere, with comparable success, including on the San Andreas and North Anatolian faults.

2. Development of geomorphic offsets and cosmogenic dating of depositional surfaces

The use of surface offsets to determine slip-rates requires sites where well-defined geomorphic features are first created, then passively preserved as displacement markers along the fault. At the sites that we targeted, the primary agents of landscape formation are glacial and fluvial processes, modulated by climate. Examples of the way in which left-lateral faulting and fluvial incision and deposition interact to produce datable offsets are shown in *figure 2*. The faults cut across alluvial fans along the piedmonts of mountain ranges. At the onset of warmer pluvials, debris accumulated in the ranges during previous glacial periods are transported by the streams and deposited in the fans. Ages of fan surfaces and moraines east of the Sierra Nevada in California are consistent with such a scenario [2]. In general, since fan emplacement requires time, the age obtained from cosmogenic dating of surface samples is that of abandonment. The highest abandoned fan surfaces are disrupted by motion along the fault. But these high fans rarely provide clear markers, and their ages only yield upper bounds for the intervals of motion. Opportunities for obtaining well-constrained slip-rates are thus best where fluvial action causes the formation of several inset terraces and risers.

In *figure 2*, as T3 is incised, a lower terrace (T2), bounded by a riser (T3/T2), forms. As long as the stream flows on T2, its bounding risers are subject to lateral cutting. The T3/T2 riser thus cannot act as a passive marker until T2 is abandoned, as the stream starts to incise again. Renewed incision implies that the threshold between aggradation and degradation of the streambed has been crossed, a condition likely driven by climate change. Hence, despite possible diachronism along-stream, terrace abandonment at a particular point usually represents a discrete temporal event. Once T2 is abandoned, T3/T2 starts to record displacement on the fault. The age of the T3/T2 offset is thus that of T2. If both the offset of T3/T2 and the surface exposure age of T2 are measured, one value of the slip-rate on the fault is constrained. Incision of T2 leads to the formation of another riser (T2/T1), which becomes a passive marker when T1 is abandoned. The exposure age of T1 in turn constrains that of T2/T1, hence another, independent value of the slip-rate at the same site. Such sites thus provide redundant constraints, as well as upper and lower bounds on the slip-rate. The positive correlation between age and displacement of diachronic markers can be tested, and possible variations of the rate with time, if any, detected. Finally, if the fault has a dip component of slip, both vertical and lateral displacement can be correlated with age. Generally, the displacements recorded by terrace risers are a minimum, as they can be re-worked by occasional flooding if the stream temporarily re-invades an already abandoned, upper terrace level.

The accumulation of cosmogenic nuclides in pebbles deposited on a terrace surface is given by the expression,

$$N(z,t) = N(z,0)\,\mathrm{e}^{-\lambda t} + \frac{P}{\lambda + \mu\,\varepsilon}\,\mathrm{e}^{-\mu z}\left(1 - \mathrm{e}^{-(\lambda+\mu\varepsilon)t}\right) \tag{1}$$

where $N(z,t)$ is the concentration at depth z (cm) and time t (yr), P the surface production rate (atoms g·yr^{-1}), λ the decay constant of the nuclide (yr^{-1}), ε the erosion rate (cm·yr^{-1}), μ the cosmic ray absorption coefficient (cm^{-1}), equal to ρ/Λ, where ρ is the density of the target rock (g·cm^{-3}) and Λ the absorption mean free path for interacting nuclear particles in the target rock (on order of 155 g·cm^{-2}). The term $N(z,0)$ is the concentration of the radionuclide at the start of the irradiation interval, i.e., the inherited component. The production rate, P, varies with both elevation and latitude. It is about 20 times greater at an elevation of 5 000 m at 40 °N than at sea level at the equator.

All of our age data were obtained from ^{10}Be and ^{26}Al, separated from quartz using the methods of Kohl and Nishiizumi [6]. The production rates are those of Nishiizumi [13], corrected for elevation and latitude using the scaling factors from Lal [7]. For samples collected from terrace and fan surfaces, $z = 0$. Where erosion and inheritance are negligible ($\varepsilon = 0, N(z,0) = 0$), model ages for ^{10}Be and ^{26}Al are derived from the simpler expression:

$$N(t) = \frac{P}{\lambda}\left(1 - \mathrm{e}^{-\lambda t}\right) \tag{2}$$

Pre-depositional inheritance results from cosmic-ray exposure either during transport in the fluvial system, or during exhumation of the parent bedrock [1]. The more rapidly a sample is exhumed and transported, the smaller the inherited component. An explicit treatment of the effects of inheritance in dating depositional surfaces requires subsurface sampling and reconstruction of the depth dependence of cosmogenic nuclide concentration accounting for the effects of variable inheritance [4, 15]. Subsurface sampling

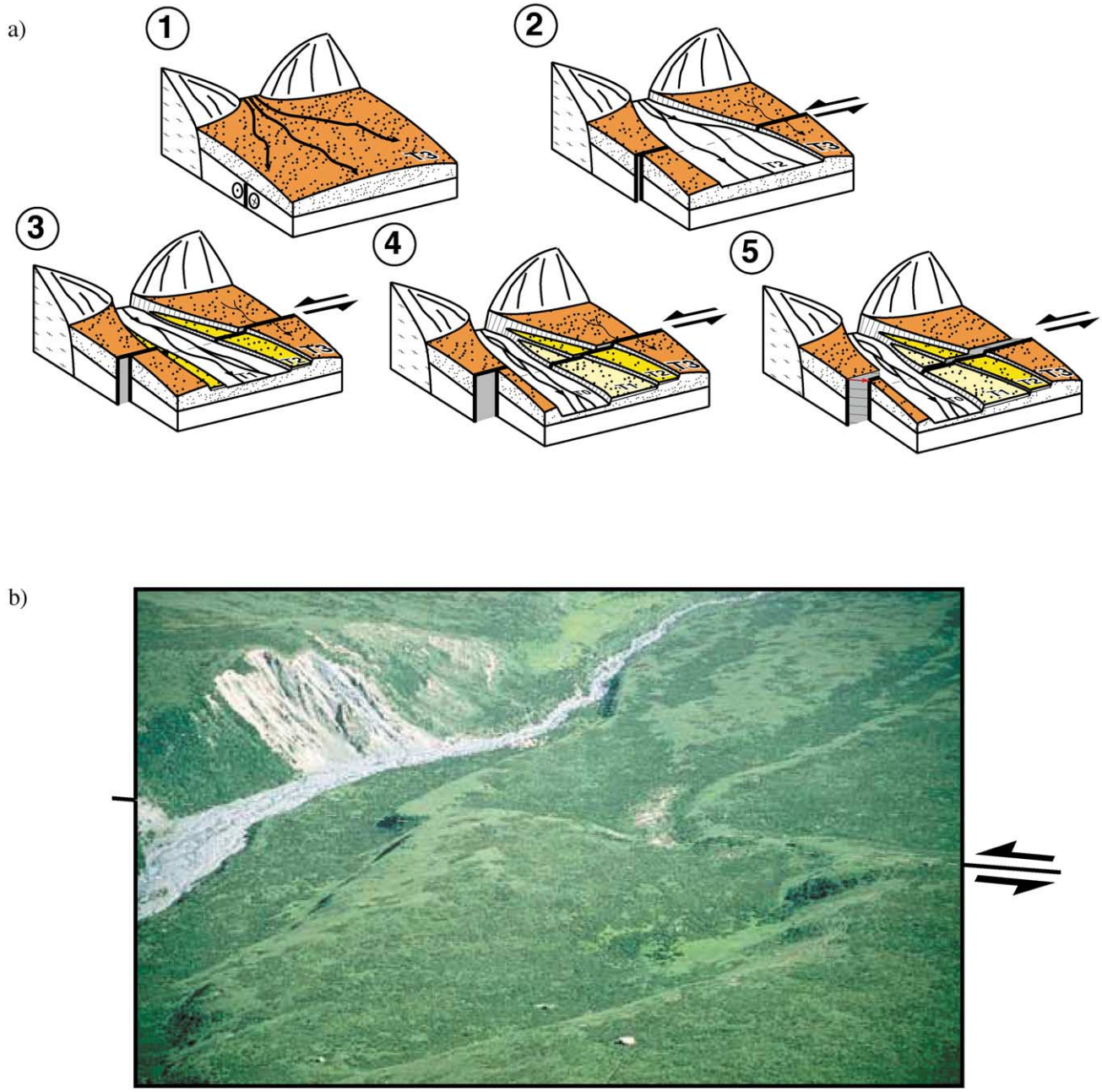

Figure 2. a. Block diagrams showing plausible sequence of terrace emplacement disrupted by strike-slip faulting across rangefront piedmont. **1.** Emplacement of large fan T3 (fill) at time of large sedimentary discharge. Fault trace is buried. **2.** Stream incises channel T2. T3 surface is abandoned and begins to record faulting, but riser is constantly refreshed by lateral cutting. **3.** During new episode of entrenchment, T2 (strath) is abandoned and riser T3/T2, now passive marker, begins to record lateral displacement. Age of T2 abandonment dates riser offset. **4.** Successive episodes of terrace beveling and entrenchment of stream lead to formation of several terraces whose risers are offset differently. **5.** Similar situation with small vertical slip component. Vertical offset accumulates when terrace is abandoned by stream. Hence vertical offset of T2 (or T1, straths) is correlated to horizontal T3/T2 (or T2/T1) riser offset, and correlated offsets have ages of T2, or T1, respectively. **b.** Example of terrace offsets along the Haiyuan left-lateral strike-slip fault. Horizontal offsets are 35 and 90 m. Photograph by F. Métivier.

Figure 2. a. Blocs diagrammes montrant une séquence de formation de terrasses alluviales recoupées par une faille décrochante. **1.** Mise en place d'un cône alluvial T3 lors d'une décharge sédimentaire importante. La faille est enfouie. **2.** La rivière creuse un lit T2. La surface T3 est abandonnée et commence à enregistrer les mouvements sur la faille, mais son bord est constamment rafraîchi par érosion latérale. **3.** Durant une nouvelle phase d'incision, T2 est abandonnée et le bord de terrasse T3/T2, devenu marqueur passif, commence à enregistrer les déplacements horizontaux. L'âge de l'abandon de T2 date le décalage du bord de terrasse. **4.** Des épisodes successifs de dépôts de terrasses et d'incision conduisent à la formation de terrasses dont les bords sont décalés différemment. **5.** Situation similaire, mais avec une composante de mouvement vertical. Le décalage vertical ne s'accumule qu'au moment de l'abandon de la surface. Ainsi, le décalage vertical de T2 (ou T1) est corrélé avec le décalage horizontal de T3/T2 (ou T2/T1) et avec l'âge de T2 (ou T1). **b.** Exemple de décalages de terrasses le long de la faille décrochante sénestre de Haiyuan. Les décalages horizontaux sont de 35 et 90 m. Photographie : F. Métivier.

was not performed in the Kunlun fault study summarized below. But the population statistics of the surface ages obtained, the steep fluvial gradient and short transport distance, the very young age of the lowest terrace in some instances, our depth-profiling results in similar environments elsewhere, and concordance with ^{14}C soil ages where possible, concur to indicate that pre-exposure in our samples was very small.

3. Concordant measurements of millennial slip rates along 600 km of the Kunlun fault

We studied three segments (Xidatan-Dongdatan, Dongxi, and Maqen) of the Kunlun fault (*figure 1*). At six sites selected with SPOT and CORONA images, and air photographs, we measured thirteen cumulative sinistral offsets of terrace risers and of a morainic ridge cut by the fault. Both ^{10}Be and ^{26}Al cosmogenic dating of quartz-rich pebbles, and radiocarbon dating of fossil organic material were used to determine the terrace surface ages. Most of the terraces we dated were straths. Hence, in general, the risers were taken to have the ages of the terraces at their base (e.g., [25]; *figure 2*). We were thus able to obtain thirteen independent, time-integrated slip rates on the fault.

The first sites, between 94 and 95 °E, span $\sim$ 50 km of the western, Xidatan-Dongdatan segment of the fault, which stretches for $\sim$ 160 km east of the Kunlun Pass, at elevations above 4 000 m (*figure 1*). In that area, the N80–90 °E striking fault-trace short-cuts the Xidatan-Dongdatan pull-apart, a narrow trough floored by coalescent alluvial fans fed by glacial streams descending from the $\sim$ 6 000 m-high Burhan Budai Shan [21]. The three sites show flights of inset terraces that rise step by step above the entrenched streams, a situation closely comparable to that schematized in *figure 2*. Large seismic mole-tracks mark the fault-trace on the ancient fans [5, 21]. Distinct terraces appear to be correlated from one site to the next, implying that they were synchronously emplaced. The terrace risers are nearly orthogonal to, hence cleanly offset by, the fault. Their offsets increase with distance from, and elevation above, the streambeds.

The site shown in *figure 3* is typical and we describe it below in some detail. There are three main terrace levels, numbered here as a function of increasing height and age. T0 is the active stream flood plain, T1′ the terrace last abandoned by the stream, T1 a first strath terrace $\sim$ 1.70 m above the stream bed, and T2 a second strath terrace, $\sim$ 2.5 m above T1. T3 is the highest level, corresponding to the ancient fan surface, about 5.5 m above T2. That surface may be in part diachronic and is incised by smaller rills, but bears no large riser in the area we sampled. Though T1 is now clearly abandoned, its western riser is not well defined, and its surface occupied by a marshy area south of the fault trace. On all the surfaces, the recent deposits are composed of relatively small, well-rounded and sorted pebbles and cobbles, at places below a thin soil and turf cover.

The principal risers (T2/T1 and T3/T2) are offset, 24 ± 3 and 33 ± 4 m, respectively, by the fault. The oldest, highest riser is offset more, as expected. The large sags and pressure ridges on T3 imply cumulative ground deformation by several earthquakes. On T2 such features are smaller and smoother. There are no clear mole tracks on T1.

For dating, we sampled fist-sized quartz pebbles, weighing $\sim$ 300 g, along two traverses parallel to the fault, up- and down-slope from it. Twenty-nine samples were processed, 13 on T1, 10 on T2 and 6 on T3. After purification of the quartz, a Be carrier was added to each sample and following HF dissolution, Al and Be were separated by ion chromatography and then converted to oxides. The aluminum concentration was determined by atomic absorption spectroscopy, and the ratios of cosmogenic ^{26}Al and ^{10}Be to stable isotopes, by accelerator mass spectrometry (AMS), at the Lawrence Livermore National Laboratory. Topographic shielding was negligible at the site. Model ages were calculated assuming zero erosion. With the exception of the youngest samples, ^{26}Al and ^{10}Be ages were concordant to within 10 %, consistent with simple exposure histories [21]. Hence, we used the mean Al–Be ages. Because the ages obtained were similar regardless of position upstream or downstream of the fault, we also grouped the sample populations from both sides of the fault.

Figure 3c shows the mean Al–Be ages of samples on each terrace, plotted in their relative position along the fault from west to east. The youngest samples (278 ± 87 yr) are found on T1, 2 m above the river-bed. We interpret these samples to reflect an exceptional flash flood that re-invaded and washed T1, re-depositing material on its surface and eroding earthquake mole tracks. Four other samples on the eastern half of that terrace yield ages that reflect its abandonment ($\sim 1\,778 \pm 388$ yr) [21].

Most sample ages on each terrace show no overlap with those on others. They tend to cluster about distinct, weighted median values ($1\,778 \pm 388$, $2\,914 \pm 471$ yr and $5\,106 \pm 290$ yr), which increase with elevation above the stream bed. But four samples are older than all the others and have experienced longer exposure histories. Such outliers appear to be reworked from older deposits up-stream. The oldest cobble ($\sim$ 22.6 kyr) likely originated in an LGM moraine ($\approx$ 20 kyr). Though we did not sample the stream bed, T0, the 278 yr-old flash-flood samples on

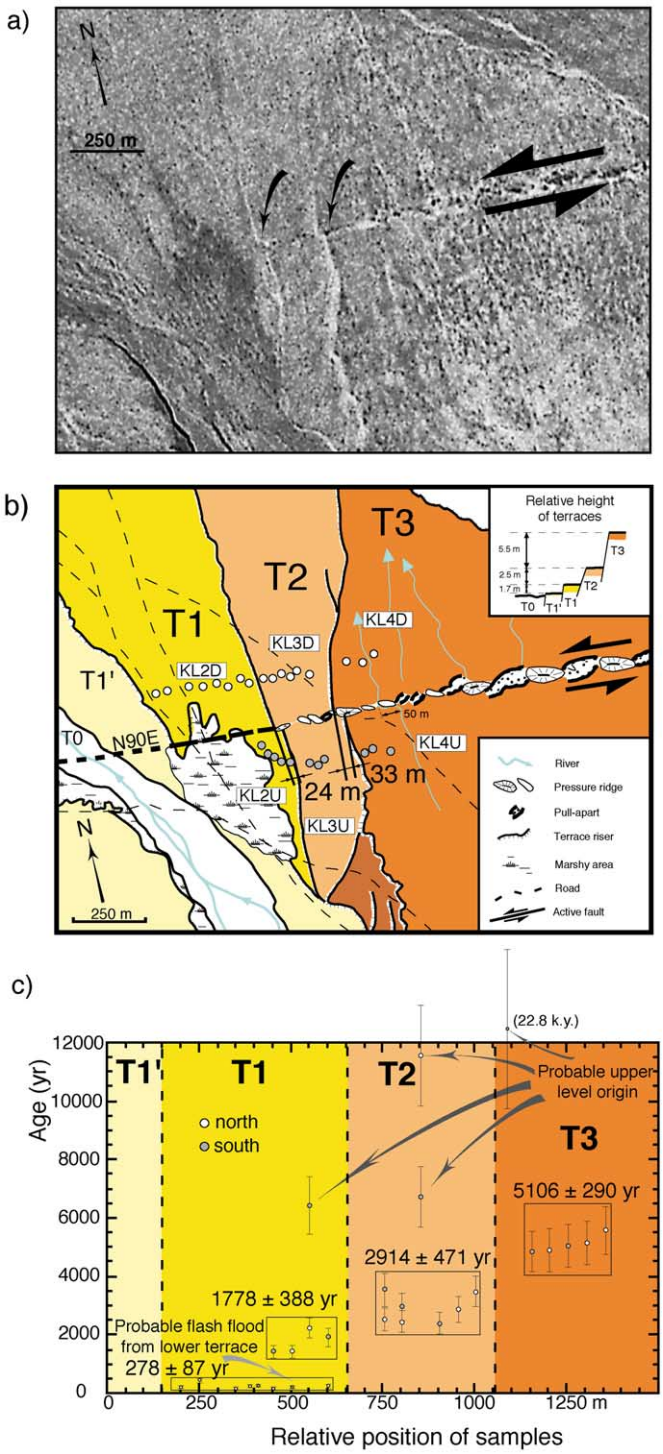

Figure 3. Site 1 along the Kunlun fault. **a.** Enlargement of CORONA satellite image DS1048-1054DA094 scanned at 2 400 dpi, with pixel size of 3.8 m. Black arrows show offsets of two principal terrace risers. **b.** Schematic interpretation of image. Quartz pebbles were sampled on top of alluvial surfaces, south (gray circles) and north (white circles) of fault trace. **c.** Plot of sample ages, for each terrace, in relative position, from west to east. For each terrace level, samples were grouped and a mean age calculated.

Figure 3. Site 1 le long de la faille du Kunlun. **a.** Agrandissment de l'image Corona DS1048-1054DA094, scannée à 2 400 dpi avec une taille de pixel de 3,8 m. Les flèches noires indiquent les décalages de deux bords de terrasses. **b.** Interprétation schématique de l'image. Des galets de quartz ont été échantillonnés à la surface des terrasses, au sud (cercles grisés) et au nord de la faille. **c.** Diagramme des âges, pour chaque terrasse, selon la position relative des échantillons d'ouest en est. Pour chaque niveau, les échantillons sont regroupés et un âge moyen est calculé.

T1 show that the inherited cosmogenic nuclide concentration is minimal, in agreement with rapid transport along the steep, small catchment between the range crest and the site. The inheritance, which appears to be at most on order of the smallest uncertainty on older ages ($\sim$ 300 yr), can thus be neglected. The millennial, left-lateral slip-rate on the fault is determined as shown in *figure 2*. It is constrained by two pairs of measurements (33 ± 4 m in 2 914 $\pm$ 471 yr, and 24 ± 3 m in 1 778 $\pm$ 388 yr) that, within error, yield consistent values of 11.3 ± 3.2 and 13.5 ± 4.6 mm·yr^{-1} (*table*, *figure 4*) [22].

The two other sites on the same segment of the fault provide measurements that corroborate those obtained at the first (*table*, *figure 4*). Overall, the 7 dated geomorphic markers at the 3 sites in Xidatan and Dongdatan constrain the slip-rate near 95 °E to be 11.7 ± 1.5 mm/yr on average (12.2 ± 1.6, 12.1

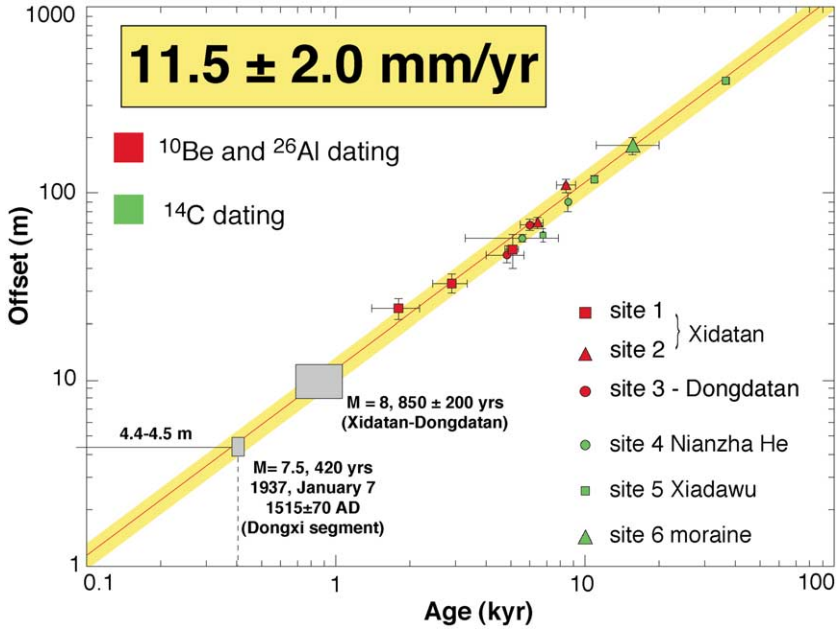

Figure 4. Summary of Late Pleistocene–Holocene left-slip rates deduced from cosmogenic ^{10}Be–^{26}Al and ^{14}C dating of alluvial terraces at six sites along the Kunlun fault. Consistency between independent values obtained with different dating techniques implies uniform average slip-rate of 11.5 mm·yr^{-1} along 600 km of fault.

Figure 4. Ensemble des vitesses de mouvement sénestre sur l'Holocène–Pléistocène supérieur, obtenues par des datations cosmogéniques ^{10}Be–^{26}Al et ^{14}C de terrasses alluviales en six sites le long de la faille du Kunlun. La cohérence des résultats obtenus avec des techniques différentes implique une vitesse uniforme de 11,5 mm·an^{-1} sur 600 km de faille.

Table. Measured offsets, with corresponding cosmogenic or ^{14}C average ages, and calculated slip rates.

Tableau. Décalages mesurés, avec les âges moyens cosmogéniques ou ^{14}C correspondants, et vitesses de glissement calculées.

Offset (m)	^{26}Al–^{10}Be age (yr)	^{14}C age (yr BP)	Slip-rate (mm·yr^{-1})
	Site 1		
24 ± 3	1 788 ± 388		13.5 ± 4.6
33 ± 4	2 914 ± 471		11.3 ± 3.2
50 ± 10	< 5 106 ± 290		> 9.8 ± 2.5
	Site 2		
70 ± 5	6 276 ± 262		11.2 ± 1.3
110 ± 10	8 126 ± 346		13.5 ± 1.8
	Site 3		
47 ± 5	4 837 ± 857		9.7 ± 2.8
68 ± 5	6 043 ± 553		11.3 ± 1.9
	Site 4		
57 ± 2		< 5 565 ± 2 245	10.3 + 7.5/ ± 2.9
90 ± 10		8 477 ± 44	10.2 ± 1.6
	Site 5		
60 ± 5		< 6 748 ± 22	8.9 ± 0.7
120 ± 5		< 11 010 ± 27	10.9 ± 0.5
400 ± 5		< 37 000 ± 900[#]	> 10.8
	Site 6		
180 ± 20	> 11 156 ± 158 and < 20 kyr		12.5 ± 3.5

[#] Uncalibrated ^{14}C age.

± 2.6, and 10.4 ± 1.1 mm·yr^{-1}, at sites 1, 2, and 3, respectively).

We studied three more sites on two other segments of the fault farther east (*figure 1*). The next two (Nianzha He, site 4, and Xiadawu, site 5) lie 20 km apart along the central, 155-km-long Dongxi–Anyemaqen segment of the fault, near 99 °E. The sites are located where the fault crosses two fluvial valleys, halfway between the 30 × 10 km, Dongxi-lake pull-apart, and the 40-km-long restraining bend of the Anyemaqen range (6 280 m). The terraces are clear straths at the former site, but fills at the latter (Xiadawu, *figure 4*). The pebbles were not quartz-rich enough for cosmogenic surface expo-

sure dating. Instead, with ^{14}C, we dated 15 charcoal pieces, two bone fragments, and freshwater shells from the uppermost gravel beneath the soil, which provided upper bounds to the terrace abandonment ages. Such ages ranged between 6 748 ± 22 and 37 000 ± 900 yr. The correlation between terraces on either side of the fault, the shapes, heights, and trends of the terrace risers, as well as the ratios between horizontal and vertical offsets on the fault were accurately constrained by 50 total-station profiles [22]. The cumulative offset values ranged from 11.3 ± 0.5 m to a maximum of 400 ± 5 m. Ultimately, the five geomorphic markers dated at the two sites that we studied on this segment of the fault yielded slip rates of 10.2 ± 1.6 and 10.9 ± 0.5 mm·yr^{-1}, comparable, within uncertainty, to the rates found ∼ 400 km to the west (*figures 1* and *4*, *table*).

Finally, near −100 °30′E, on the eastern, N110 °E-striking Maqen segment of the fault (*figure 1*), the main fault-strand offsets by 180 ± 20 m a low-level lateral moraine (site 6, *table*). Protruding surface boulders, and the fresh shape of the morainic ridge were indicative of its emplacement during the Last Glacial Maximum (∼ 20 ka BP in northern Tibet, e.g. [20]), at the time of farthest advance of the glacier. The highest outwash terrace dammed behind the offset moraine yielded a ^{14}C age of 11 156 ± 157 yr BP (*table*), implying a slip-rate of 12.5 ± 2.5 mm·yr^{-1}, similar to those found at the first five sites (*figure 4*). The average slip rate along the length of fault spanned by our sites is thus 11.5 ± 2 mm·yr^{-1} [22] (*figure 4*).

4. Characteristic coseismic slip and recurrence time of similar earthquakes

In Xidatan and Dongdatan, the smallest visible offsets of the youngest geomorphic features such as small rills or low-level risers ranged between 8 and 12 m, compatible with those (∼ 10 m) found by Kidd and Molnar [5] and Zhao [27]. We also measured 18 multiple offset values 2 or 3 times greater than these minimum offsets. The minimum values, which vary by less than 20 % from place to place, thus likely represent the coseismic surface-slip of large, similar events. Clearly, two and three $M \approx 8$ earthquakes, each with 10–12 m of slip, account for the offsets of the T2/T1 and T3/T2 risers at site 1 in the last ∼ 1 800 and ∼ 2 900 yr, respectively (*figure 3*). The ∼ 50 m gully offset and the large sag-ponds and pressure-ridges on T3 (*figure 3*) probably result from five such earthquakes in the last ∼ 5 200 yr. Such quantitative evidence implies that the Xidatan–Dongdatan segment of the Kunlun fault ruptures during similar, great ($M \approx 8$) earthquakes with characteristic slip (Δu = 10.5 ± 1.5 m) and a recurrence time Tr on order of 850 ± 200 yr (*figure 4*) [21].

We found a similar situation on the Dongxi–Anyemaqen segment of the fault, which is marked by the mole tracks of the 7 January 1937 $M = 7.5$ earthquake. Fourteen total-station profiles of offset rills on the lowest Nianzha He terrace (T′0, *figure 5*) show two statistically different clusters of coherent horizontal and vertical offset values, each with $\Delta h \approx 11\Delta v$. This implies two distinct events, each with $\Delta h \approx 4.4 \pm 0.4$ m and $\Delta v \approx 0.4 \pm 0.1$ m. Thus not only did the rills record the last (1937) and penultimate earthquakes, but these two events had identical slip. The 11.3 m offset of the T1/T′0 riser, now degraded by uneven colluvial collapse, may attest to three such events ($3 \times 4.4 = 13.2$ m). Earthquakes with characteristic slip thus also appear to rupture this segment of the fault. But their sizes and repeat times are different from those in Xidatan. At Nianzha He, the 1937, $M \approx 7.5$ earthquake, with $\Delta h \approx 4.4 \pm 0.4$ m and $\Delta v \approx 0.4 \pm 0.1$ m, appears to be typical. Given the slip rate (10.3 mm·yr^{-1}), such $M \approx 7.5$ earthquakes appear to recur about every 420 yr, with previous events in 1 515 ± 70 AD (*figure 4*) and 1 095 ± 140 AD, and the next due around 2 350 AD [22].

5. Discussion and conclusion

Thirteen distinct geomorphic offsets dated with three different techniques at six sites constrain the slip-rate on the Kunlun fault to be uniform (11.5 ± 2 mm·yr^{-1}; *figure 1*), and constant over a time-span of about 40 000 yr, for a distance of 600 km. On two segments, the regular recurrence ($Tr \approx 420$ and 850 yr) of earthquakes of different size ($M \approx 7.5$ and 8), but with characteristic slip, appears to typify the behaviour of the fault in the last few thousand years. Our data is thus an essential step to assess the average length of the seismic cycle, and the maximum size of recent events on these two segments. Recurrent offsets mapped elsewhere on SPOT images suggest that it is possible to extrapolate the rate constrained in the field at a few sites to much of the fault-length (≈ 1 200 km). A uniform rate over such a distance is plausible since, unlike other Central Asian faults (e.g., [12]), the Kunlun fault does not splay into oblique strands.

Application of the same technique to the other two principal left-slip faults of northern Tibet has been equally successful. On the Haiyuan fault (*figures 1* and *2*), ^{10}Be–^{26}Al surface exposure ages of glacial moraines in the Lenglong Ling range, in the west, and ^{14}C dating of fluvial terrace risers near Songshan, in the east, constrain two slip-rate values: 20 ± 5 and

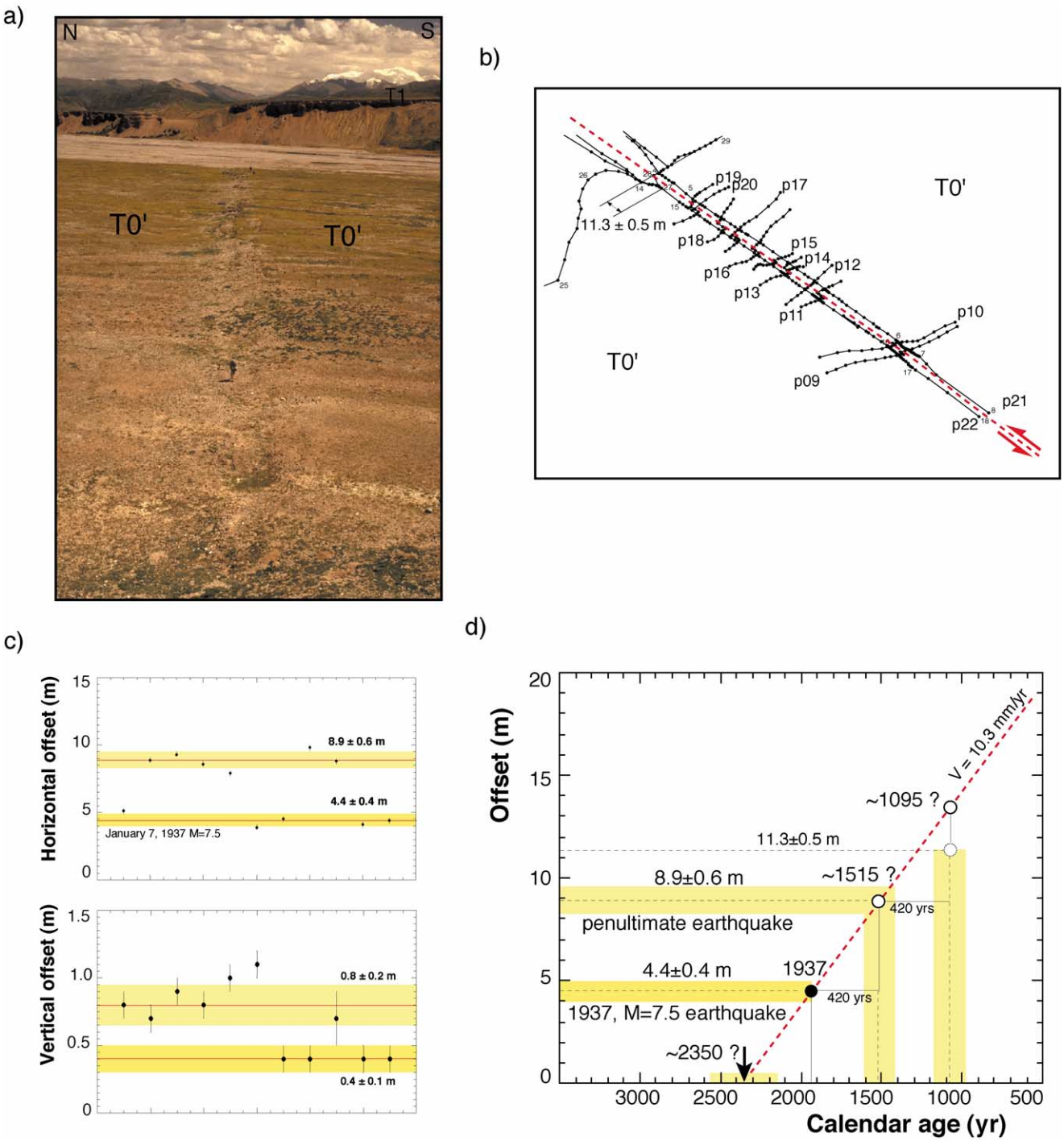

Figure 5. a. View of disrupted terrace surface at Nianzha He site (site 4) along Kunlun Fault. 1937 and penultimate earthquakes have offset small rill channels incised in terrace surface. **b.** Map view of profiles leveled in the field along channels and risers. **c.** Horizontal and vertical offsets of channels. Two sets of offsets (4.4/0.4 and 8.9/0.8) indicate displacements during the last and penultimate events. **d.** Long term slip rate and offset measurements imply a recurrence time of 420 years for events with a slip of 4.4 m.

Figure 5. a. Vue d'une terrasse recoupée par la faille du Kunlun au site Nianzha He (site 4). Les tremblements de terre de 1937 et le précédent ont décalé de petits chenaux incisés à la surface de la terrasse. **b.** Carte des profils topographiques relevés le long des chenaux et terrasses. **c.** Décalages horizontaux et verticaux des chenaux. Les deux ensembles de décalages (4,4/0,4 et 8,9/0,8) indiquent que les deux derniers événements ont des déplacements semblables. **d.** La vitesse à long terme et les mesures des décalages permettent de déterminer un temps de récurrence de 420 ans pour des événements au déplacement de 4,4 m.

12 ± 4 mm·yr^{-1}, averaged over time spans of about 11 000 and 14 000 years, respectively. The westward increase is due to the contribution of the Gulang fault, another important left-lateral fault that splays northeastwards off the Haiyuan fault between the two sites (*figure 1*). Similar, large earthquakes with $M_w \geqslant 8$ and characteristic slip $\Delta u = 12 \pm 4$ m appear to recur every $1\,050 \pm 450$ yr at the eastern site [3, 8, 9].

The study of the Altyn Tagh fault, a particularly daunting task in view of its great length ($\sim 2\,000$ km), has also begun to provide long-awaited results, critical to a quantitative understanding of continental deformation. The slip rate decreases at either end of the main strand of the fault, due to splaying sinistral faults and thrusts that take up part of the movement. But the central part of the fault, between 83 and 94 °E, slips at rates of 2 to 3 cm·yr^{-1}, comparable to that of the San Andreas fault, in California. Near Aksay, at 94 °E (*figure 1*), multiple terrace riser offsets whose minimum and maximum ages are constrained both with ^{10}Be–^{26}Al exposure ages and ^{14}C dating yield a slip-rate of 23 ± 8 mm·yr^{-1} in the last 6 000 yr [10]. East and west of Tura (~ 87 °E), at two distinct sites, one fluvial, the other glacial, the same combination of techniques yields a rate of 31 ± 6 mm·yr^{-1}, constrained by nine independent pairs of offsets and ages [11]. At the glacial site, we were able to show that this slip-rate has remained constant for at least 110 000 yr, the longest time interval we could document so far. During that period, the fault has displaced the principal glacial catchment of the Sulamu range by as much as 3.6 km, providing a unique example of the interaction between strike-slip faulting and ice-stream advance and retreat. With regard to the kinematics and mechanics of continental deformation, such results establish that, near Tura, the Altyn Tagh fault absorbs more than one third of the convergence between India and Asia, at a rate comparable to that of major transform plate-boundaries.

Overall, our study demonstrates that quantitative 'morphochronology', based on the new technique of cosmogenic surface exposure dating, is an unparalleled tool to determine long-term slip-rates on active faults. When combined with single event coseismic slip-amounts, such slip rates give access to the first order parameters of the seismic cycle: its length, its regularity and the sizes of typical earthquakes that rupture the fault at the sites targeted. Furthermore, on the Haiyuan fault, our work has led to the identification of a 220-km-long seismic gap, the Tianzhu gap, which appears to have been quiescent since the 4th century AD. The fact that fault segments adjacent to this gap ruptured during two great earthquakes in 1920 and 1927, and that the surrounding regions were shaken by more events with $5 \leqslant M \leqslant 6$ since 1986 than in the 50 years prior to that date, has led us to forecast the impending occurrence of a $M > 8$ earthquake, whose coseismic slip might exceed 15 m [3, 8], along that gap.

In several instances, our measurements support the view that certain earthquakes on specific segments of the faults repeat with surprisingly similar rupture parameters. Well-documented examples of this type of behaviour are still rare, and limited to a few faults that slipped during recent earthquakes, especially in California (e.g., Superstition Hills, 1987, and Imperial faults, 1940, 1979 [18]). Besides, it has been difficult to compare coseismic slip-amounts and rupture lengths for more than a few earthquakes. But the emerging picture, supported in particular by the similarities and differences between the breaks of the 1940 and 1979 earthquakes on the Imperial fault, appears to be one in which large earthquakes result from the failure of fault patches whose individual slip functions are roughly invariant [18]. Not all earthquakes are the same through consecutive cycles, because they may not rupture the same adjacent patches or segments (*figure 6*). But the persistence of similar slip functions indicates that they are controlled by invariant physical properties, such as patch strength and friction law parameters [23]. Introducing such parameters in physical rupture models makes it possible, in turn, to simulate synthetic calendars of events over thousands of years, with particularly realistic results (e.g., Imperial fault, [23], *figure 6*; San Francisco Bay area, [24]). It is thus vital to quantify rupture parameters for sequences of earthquakes as long as possible, on many more faults.

From a methodological standpoint, the excellent agreement we obtained, where feasible, between ^{14}C dating and combined ^{10}Be–^{26}Al surface exposure ages (*figure 4*), and the negligible perturbation of cosmogenic nuclide systematics by inheritance or post-depositional disturbance, confirm the reliability of the latter technique. Its use is not as straightforward as it seems, however, and there are clear pitfalls to avoid. What makes the dating strategy we implemented successful, and the results robust, is the concordance of the cosmogenic model ages determined with both ^{10}Be and ^{26}Al, and the collection of sufficiently numerous samples on paired offset terraces on either side of the faults. This allows both statistical treatment of individual measurements, as in paleomagnetic studies, and unambiguous assessment of the correspondence between terraces. Rejection of outliers with complex exposure histories or provenance would be impossible otherwise. For this reason, inferences based on small sample numbers and one cosmogenic isotope only (e.g., [16, 17]), as well as speculations about landscape evolution deduced from them, should be viewed with cau-

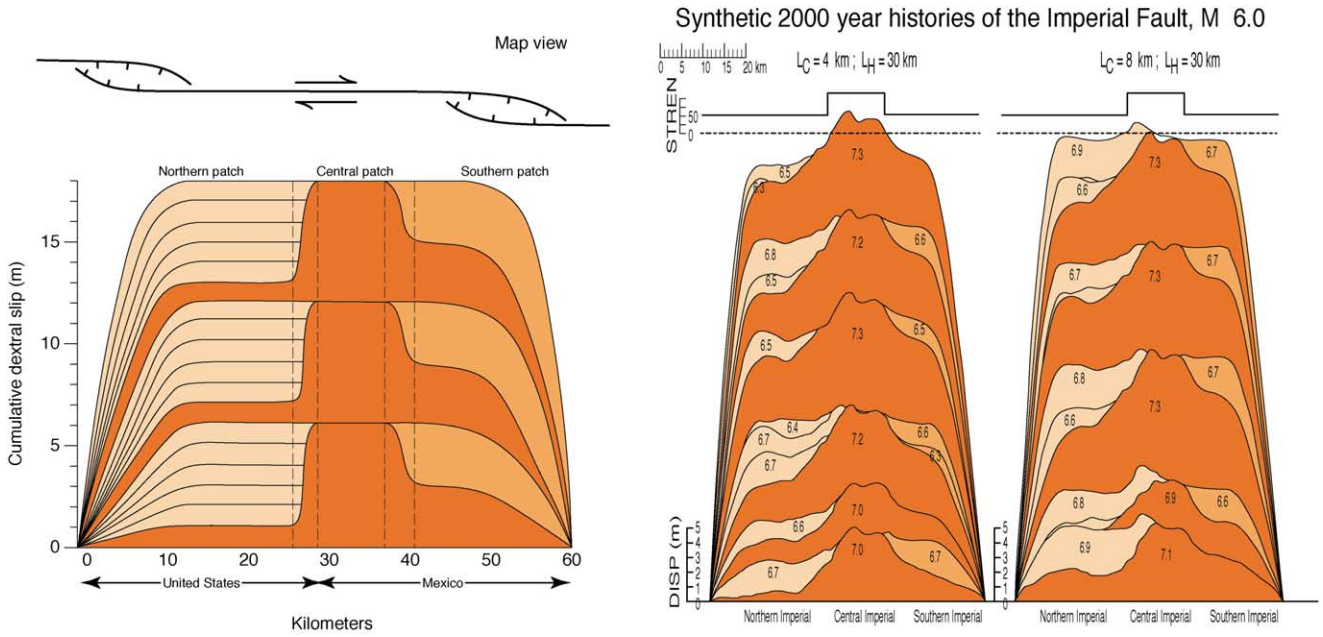

Figure 6. Left. Conceptual 'slip-patch' rupture scenario for the long-term behaviour of Imperial fault, California, after [18]. This scenario is based on the coseismic slip distributions measured along strike during the 1940 (orange), and 1979 (light beige) earthquakes, and on the assumption of uniform long-term slip along strike. Each patch, corresponding to a segment at the surface, has its own invariant, hence characteristic, slip-function. The transitions between the three patches are narrow, and reflect permanent differences in strength. **Right.** Two examples of synthetic, 2 000-year-long, computer-simulated seismic histories of the Imperial fault, based on the 1940 and 1979 observations, after [23]. The piles with recurrent colors represent cumulative slip from earthquakes with $M \geqslant 6$. The small numbers indicate the magnitude of each earthquake. The strengths of the patches (above) are in bars. Modest differences in the friction law parameters (L_C: minimum patch length for failure; L_H: maximum rupture length prior to healing) result in different magnitude variations on each segment.

Figure 6. Gauche. Scénario conceptuel (*characteristic slip patch rupture*) du fonctionnement sismique long terme de la faille Impériale, en Californie, d'après [18]. Ce scénario se fonde sur les distributions de glissement cosismique mesurées le long des trois segments de la faille lors des séismes de 1940 (orange) et de 1979 (beige clair), ainsi que sur l'hypothèse d'une vitesse de glissement long terme uniforme. Chaque *patch* possède sa propre distribution de glissement, invariante d'un séisme à l'autre, donc « caractéristique ». Les transitions entre les trois *patches*, qui correspondent en surface aux segments, sont abruptes, et reflètent donc des différences permanentes de résistance mécanique. **Droite.** Deux exemples de catalogues sismiques synthétiques, longs de 2 000 ans, sur la faille Impériale, basés sur les observations faites lors des séismes de 1940 et 1979, d'après [23]. Les empilements de plages de couleurs récurrentes représentent le glissement cumulé de séismes de magnitudes $\geqslant 6$. La magnitude de chaque séisme est indiquée par le chiffre en minuscules. La résistance mécanique de chaque *patch* est donnée, en bars, sur le graphe au-dessus. Des différences modestes des paramètres de friction (L_C : longueur minimum du *patch* de rupture ; L_H : longueur maximum de rupture avant « cicatrisation ») conduisent à des variations différentes des magnitudes sur chaque segment.

tion. An additional result of our work is to demonstrate that the landforms of northeastern Tibet are principally shaped by climatic changes, whose effects can be read and correlated from place to place. It is now beyond doubt that the clearest, and most abundant, fluvial and glacial markers formed during the most recent interglacials (or interstadials) and glacial maxima, respectively, as we suggested long ago.

Whether the long-term geomorphic 'memory' and response to climate and tectonics at lower elevations can be deciphered as well remains to be demonstrated. But studying the San Andreas fault in California, or the North Anatolian fault in Turkey with the tools that have helped us quantify the 10–100 ka behaviour of Asian faults, promises to be a fruitful endeavor, since quantitative knowledge of these faults is for now limited to the last few thousand years.

In any case, coupling morphochronology with paleo-seismological trenching should clearly be at the core of any attempt to understand active fault behaviour, estimate long-term seismic hazard and, through simulation, pave the way towards earthquake forecast. Both techniques are at the forefront of quantitative geology, rather than of seismology. But the questions they can address and solve, particularly concerning past and future earthquake calendars, are the very first ones one should seek to answer in any region of active faulting, whether or not there is remembrance of it being shaken in the historical past.

Acknowledgements. Various parts of the long-term studies summarized here have involved many more essential collaborators than there are co-authors of this paper. We are indebted to all of them, particularly, Y. Gaudemer, B. Meyer, G. King, R. Finkel, M. Caffee, M. Kashgarian, Zhao

Guoguang, Xu Zhiqin, Xu Xiwei, Liu Baichi, Yuan Daoyang, and Lu Taiyi. We had fruitful discussions also with R. Armijo, F. Metivier, G. Peltzer, and J.-P. Avouac, whose comments helped improve the paper. We gratefully acknowledge constant financial support from the 'Institut national des sciences de l'Univers' (PNRN and IT programs), the 'Centre national de la recherche scientifique', Paris (France), and the Lawrence Livermore National Laboratory, Livermore (California). We also thank the China Seismological Bureau and the Ministry of Lands and Resources in Beijing (China) for the excellent logistical support provided in the field year after year. This is IPGP contribution # 1779.

References

[1] Anderson R.S., Repka J.L., Dick G.S., Explicit treatment of inheritance in dating depositional surfaces using in situ ^{10}Be and ^{26}Al, Geology 96 (1996) 47–51.

[2] Bierman P.R., Gillespie A.R., Caffee M.W., Cosmogenic ages for earthquake recurrence intervals and debris flow fan deposition, Owens Valley, California, Science 270 (1995) 447–450.

[3] Gaudemer Y., Tapponnier P., Meyer B., Peltzer G., Guo Shunmin, Chen Zhitai, Dai Huagung, Cifuentes I., Partitioning of crustal slip between linked, active faults in the eastern Qilian Shan, and evidence for a major seismic gap, the 'Tianzhu gap', on the Western Haiyuan Fault, Gansu (China), Geophys. J. Int. 120 (1995) 599–645.

[4] Hancock G.S., Anderson R.S., Chadwick O.A., Finkel R.C., Dating fluvial terraces with ^{10}Be and ^{26}Al profiles: application to the Wind River, Wyoming, Geomorphology 27 (1999) 41–60.

[5] Kidd W.S.F., Molnar P., Quaternary and active faulting observed on the 1985 Academia Sinica-Royal Geotraverse of Tibet, Phil. Trans. R. Soc. London A 327 (1988) 337–363.

[6] Kohl C.P., Nishiizumi K., Chemical isolation of quartz for measurement of in situ produced cosmogenic nuclides, Geochim. Cosmochim. Acta 56 (1992) 3583–3587.

[7] Lal D., Cosmic ray labeling of erosion surfaces: in situ nuclide production rates and erosion models, Earth Planet. Sci. Lett. 104 (1991) 424–439.

[8] Lasserre C., Morel P.-H., Gaudemer Y., Tapponnier P., Ryerson F.J., King G., Métivier F., Kasser M., Kashgarian M., Baichi L., Taiyi L., Daoyang Y., Post-glacial left slip-rate and past occurrence of $M \geqslant 8$ earthquakes on the western Haiyuan fault (Gansu, China), J. Geophys. Res. 104 (1999) 17633–17651.

[9] Lasserre C, Gaudemer Y., Tapponnier P., Mériaux A.-S., Van der Woerd J., Ryerson R., Yuan Daoyang, Late Pleistocene slip-rate on the Leng Long Ling segment of the Haiyuan fault, Qinghai, China, using in situ ^{10}Be and ^{26}Al cosmogenic nuclides dating, Geophys. J. Int. (in press).

[10] Mériaux A.-S., Tapponnier P., Ryerson F.J., Van der Woerd J., King G., Finkel R.C., Caffee M.W., Application of cosmogenic ^{10}Be and ^{26}Al dating to neotectonics of the Altyn Tagh in central Asia (Gansu, China), EOS Trans. AGU Fall Meeting (Suppl.) 78 (1997) 46.

[11] Mériaux A.-S., Ryerson F.J., Tapponnier P., Vanderwoerd J., Finkel R., Caffee M., Lasserre C., Xu Xiwei, Li Haibing, Xu Zhiqin, Fast extrusion of the Tibet Plateau: a 3 cm/yr, 100 kyr slip-rate on the Altyn Tagh Fault, EOS Trans. AGU Fall Meeting (Suppl.) 81 (2000) 48.

[12] Meyer B., Tapponnier P., Bourjot L., Métivier F., Gaudemer Y., Peltzer G., Shunmin G., Zhitai C., Crustal thickening in Gansu-Qinghai, lithospheric mantle subduction, and oblique, strike-slip controlled growth of the Tibet plateau, Geophys. J. Int. 135 (1998) 1–47.

[13] Nishiizumi K., Cosmic-ray production rate of ^{10}Be and ^{26}Al in quartz from glacially polished rocks, J. Geophys. Res. 94 (1989) 17907–17915.

[14] Peltzer G., Tapponnier P., Gaudemer Y., Meyer B., Guo Shunmin, Yin Kelun, Chen Zhitai, Dai Huagung, Offsets of Late Quaternary morphology, rate of slip, and recurrence of large earthquakes on the Chang Ma fault (Gansu, China), J. Geophys. Res. 93 (B7) (1988) 7793–7812.

[15] Repka J.L., Anderson R.S., Finkel R.C., Cosmogenic dating of fluvial terraces, Fremont River, Utah, Earth Planet. Sci. Lett. 152 (1997) 59–73.

[16] Ritz J.F., Brown E.T., Bourlès D.L., Philip H., Schlupp A., Raisbeck G.M., Yiou F., Enkhtuvshin B., Slip-rates along active faults estimated with cosmic-ray-exposure dates: application to the Bogd fault, Gobi-Altaï, Mongolia, Geology 23 (1995) 1019–1022.

[17] Siame L.L., Bourlès D.L., Sébrier M., Bellier O., Castano J.-C., Araujo M., Perez M., Raisbeck G.M., You F., Cosmogenic dating ranging from 20 to 700 ka of a series of alluvial fan surfaces affected by the El Tigre fault, Argentina, Geology 25 (1997) 975–978.

[18] Sieh K., The repetition of large-earthquake ruptures, Proc. Natl. Acad. Sci. 93 (1996) 3764–3771.

[19] Sieh K., Jahns R.H., Holocene activity of the San Andreas fault at Wallace Creek, California, Geol. Soc. Am. Bull. 95 (1984) 883–896.

[20] Thompson L.G., Yao T., Davis M.E., Henderson K.A., Mosley-Thompson E., Lin P.-N., Beer J., Synal H.-A., Cole-Dai J., Bolzan J.F., Tropical climate instability: the last glacial cycle from a Qinghai–Tibetan ice core, Science 276 (1997) 1821–1825.

[21] Van Der Woerd J., Ryerson F.J., Tapponnier P., Gaudemer Y., Finkel R., Mériaux A.S., Caffee M., Zhao Guoguang, He Qunlu, Holocene left slip-rate determined by cosmogenic surface dating on the Xidatan segment of the Kunlun fault (Qinghai, China), Geology 26 (1998) 695–698.

[22] Van der Woerd J., Ryerson F.J., Tapponnier P., Mériaux A.-S., Gaudemer Y., Meyer B., Finkel R.C., Caffee M.W., Zhao G., Zhiqin X., Uniform slip-rate along the Kunlun fault: implication for seimic behaviour, large-scale tectonics and climatic imprint on Tibetan landforms, Geophys. Res. Lett. 27 (2000) 2353–2356.

[23] Ward S.N., Dogtails versus rainbows: synthetic earthquake rupture models as an aid in interpreting geological data, Bull. Seismol. Soc. Am. 87 (1997) 1422–1441.

[24] Ward S.N., San Francisco bay area earthquake simulations: a step toward a standard physical earthquake model, Bull. Seismol. Soc. Am. 90 (2000) 370–386.

[25] Weldon R.J., Sieh K.E., Holocene rate of slip and tentative recurrence interval for large earthquakes on the San Andreas fault in Cajon Pass, southern California, Geol. Soc. Am. Bull. 96 (1985) 793–812.

[26] Zhang P., Molnar P., Zhang M., Deng Q., Wang Y., Burchfiel B.C., Song F., Royden L.H., Jiao D., Bounds on the recurrence intervals of major earthquakes along the Haiyuan fault in north-central China, Seism. Res. Lett. 59 (1988) 81–89.

[27] Zhao G., Quaternary faulting in north Qinghai–Tibet plateau, Continental dynamics, Institute of Geology, Beijing 1 (1996) 30–37.